INSTITUTE OF PHYSICS PUBLISHING JOURNAL OF PHYSICS D: APPLIED PHYSICS

J. Phys. D: Appl. Phys. **39** (2006) 3362–3370 doi:10.1088/0022-3727/39/15/021

Thermal characterization of micro/nanoscale conductive and non-conductive wires based on optical heating and electrical thermal sensing

Jinbo Hou, Xinwei Wang[1] and Jiaqi Guo

Department of Mechanical Engineering, N104 Walter Scott Engineering Center, University of Nebraska–Lincoln, Lincoln, NE 68588-0656, USA

E-mail: xwang3@unl.edu

Received 15 March 2006, in final form 12 May 2006
Published 21 July 2006
Online at stacks.iop.org/JPhysD/39/3362

Abstract

In this work, a technique based on optical heating and electrical thermal sensing (OHETS) is developed to characterize the thermophysical properties of one-dimensional micro/nanoscale conductive and non-conductive wires. In this method, the to-be-measured thin wire is suspended over two electrodes and is irradiated with a periodically modulated laser beam. The laser beam induces a periodical temperature variation in the wire/tube, which will lead to a periodical change in its electrical resistance. A dc current is applied to the sample, and the resulting periodical voltage variation over the wire is measured and used to extract the thermophysical properties of the wire/tube. A 25.4 μm thick platinum wire is used as the reference sample to verify this technique. Sound agreement is obtained between the measured thermal conductivity and the reference value. Applying the OHETS technique, the thermal diffusivity of conductive single-wall carbon nanotube (SWCNT) bundles and non-conductive human hair and cloth fibres are measured. For non-conductive wires, a thin (∼nm) metallic film is coated at the outside of the wire for electrical thermal sensing. The measured thermal diffusivities for three different SWCNT bundles are 2.98×10^{-5} m^2 s^{-1}, 4.41×10^{-5} m^2 s^{-1} and 6.64×10^{-5} m^2 s^{-1}. These values are much less than the thermal diffusivity of graphite in the layer direction. For human hair and microscale cloth fibres, our experiments show that their thermal diffusivities are at the level of 10^{-6} m^2 s^{-1}.

1. Introduction

In recent years, due to the demand for developing reliable microelectromechanical systems (MEMS) and nanoelectromechanical systems (NEMS), characterizing the thermophysical properties of different materials at micro/nanoscales has received considerable attention. In the past, transient thermoreflectance (TTR) [1], 3ω [2], photothermal deflection (PTD) [3] and photoacoustic (PA) [4] methods have been well developed to measure the thermal properties of thin films. For investigation of the thermophysical properties of one-dimensional micron/nanostructures, limited experimental approaches have been developed. At present, the 3ω method [5,6] and microfabricated devices method [7,8] are the main measurement techniques to obtain thermophysical properties of materials in such low dimensions and small scales.

Because the thermophysical properties of carbon nanotubes (CNTs) are of fundamental interest and play a critical role in controlling the performance and stability of CNT devices [9], a large number of theoretical and experimental investigations have been conducted to understand the thermophysical properties of CNTs. The experimental

[1] Author to whom any correspondence should be addressed.

studies of thermophysical properties of CNTs have increased with the advances in nanotube synthesis. For single-wall carbon nanotube (SWCNT) bundles, Hone *et al* [10, 11] by using a comparative method conducted a series of experiments to measure the thermal conductivity. They reported that the thermal conductivity increased smoothly with temperature increasing from 10 to 400 K. At room temperature, thermal conductivity of 35 and 218 $\mathrm{W\,m^{-1}\,K^{-1}}$ were obtained for different SWCNTs samples in their work. Later, a comparative steady-state method was used to study SWCNT filled with C_{60} by Vavro *et al* [12]. Their result showed that at room temperature the thermal conductivity of SWCNTs filled with C_{60} was $\sim$15 $\mathrm{W\,m^{-1}\,K^{-1}}$. Recently, one-dimensional SWCNT bundles and individual SWCNTs were investigated by Shi *et al* [8] and Yu *et al* [13]. In their work, a suspended microfabricated device was employed. At room temperature, thermal conductivities of $\sim$3 and $\sim$150 $\mathrm{W\,m^{-1}\,K^{-1}}$ for SWCNT bundles of 148 and 10 nm diameters were reported in the work of Shi *et al* [8]. In the work of Yu *et al* [13], a much larger value of $\sim$3000 $\mathrm{W\,m^{-1}\,K^{-1}}$ was reported. For a multi-wall carbon nanotube (MWCNT), Xie *et al* [14], Yi *et al* [15] and Lu *et al* [5] studied the thermal conductivity of MWCNT bundles by employing the 3ω method. A conventional laser-flash method was used by Zhang *et al* [16] to measure the thermal conductivity of MWCNT bulk material. Recently, thermal conductivity of individual MWCNTs was investigated by a microfabricated suspended device (Kim *et al* [7]), non-contact photothermal experiment (Wang *et al* [17]), 3ω method (Choi *et al* [18]) and a temperature sensing scanned microscope probe (Brown *et al* [19]).

For the techniques reviewed above, the 3ω method provides a compelling means of characterizing the thermal conductivity of CNTs with sound accuracy. On the other hand, this technique requires that the sample is conductive and endowed with linear I–V behaviour in the applied ac voltage range. Meanwhile, CNTs have both metallic and semiconducting properties, depending on their chirality indexes (n, m). A layer in the MWCNT will have metallic conduction when the difference between the two indexes (n and m) is divisible by three (Dresselhaus *et al* [9]). Otherwise, the layer will be semiconducting, leading to a non-linear I–V relationship. As a result, the 3ω technique can only be applied to metallic CNTs.

Motivated to solve the problem described above, in this paper, a technique based on optical heating and electrical thermal sensing (OHETS) and the associated analytical solution for investigating the thermophysical properties of one-dimensional micro/nanostructures are developed. This technique can be applied to both conductive and non-conductive materials. By employing a modulated laser beam as the heating source and detecting the periodic resistance change in the sample, the thermophysical properties of 1D single conductive wires/tubes can be extracted. For non-conductive wires/tubes, a thin Au film is coated at the outside of the wire for transient electrical thermal sensing. To test this technique, thermal conductivity measurement of platinum wire specimens is performed. By applying this technique, the thermal diffusivities of three different SWCNT bundles, human hair and cloth fibres are measured successfully. In section 2, the experimental principle and physical model development are presented. The experimental details and results are discussed in section 3.

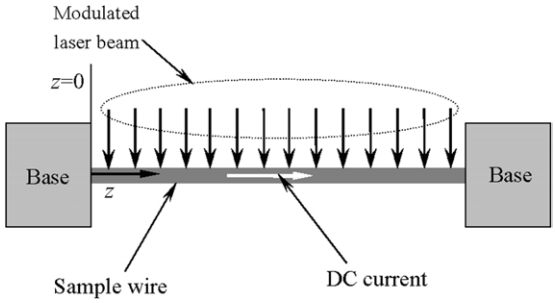

Figure 1. Schematic of the experimental principle for the OHETS technique.

2. Experimental principle and physical model development

2.1. Experimental principle

In the OHETS experiment, the to-be-measured wire is suspended between two copper electrodes. The wire is irradiated with a periodically modulated laser beam as shown in figure 1. The laser spot is large enough to cover the entire wire and a portion of the bases. Upon periodical laser heating, the wire will experience a periodical temperature change with time. As a result, the resistance of the wire will change with time periodically. In the experiment, the dimensions of the bases are much larger than the diameter of the wire, ensuring that the temperature change of the bases directly from the laser heating is much smaller in comparison with that of the wire. In addition, the electrical resistances of the electrode bases are much smaller than that of the wire. As a result, the resistance variation of the bases due to laser irradiation will be negligible compared with that of the thin wire.

In order to detect the resistance variation of the wire, a dc current is passed through the wire. The dc current and the periodical resistance variation of the wire will produce a periodical voltage variation over the wire with the same frequency of the modulated laser beam. The heat conduction along the thin wire strongly affects the temperature variation along the wire which will be probed by measuring the voltage variation. The phase shift of the voltage variation relative to the laser beam can be used to determine the thermophysical properties of the sample. In the experiment, a series of frequencies is chosen to measure the phase shift and conduct the fitting. The modulation frequency of the laser irradiating the wire will be carefully selected to make the thermal diffusion length $\mu = \sqrt{2\alpha/\omega}$ (α: thermal diffusivity of the wire; ω: modulation frequency) much larger than the wire diameter D. As a result, it is physically reasonable to assume that the wire has a uniform temperature distribution in its cross-section. Consequently, only the heat transfer along the axial direction of the wire needs to be considered.

2.2. Physical mode development

The heat transfer of interest will be divided into two parts: one part is the heat transfer along the wire (z direction as

shown in figure 1), and the other part is the heat transfer in the bases. Solutions to these two parts will be combined using the boundary conditions at the interface ($z = 0$) between the wire and the base. In the experiment, the laser heating power has the form of $I = I_0(1 + \cos(\omega t))/2$. For the heat transfer in the wire along the axial direction, the governing equation, in the complex form, is

$$\frac{\partial(\rho c_p T)}{\partial t} = k\frac{\partial^2 T}{\partial z^2} + Q_0 e^{i\omega t} + Q_0, \tag{1}$$

where $Q_0 = E/LS$, L and S are the length and cross-sectional area of the wire, respectively. E is the laser beam energy absorbed by the wire. ρ, c_p and k are the density, specific heat and thermal conductivity of the wire, respectively. It needs to be pointed out that in equation (1) the laser beam is assumed uniform over the wire. In fact, there is a distribution of the laser beam along the axial direction of the wire. The effect of the non-uniformity of the laser beam is discussed in the next section.

The solution to the above thermal diffusion equation consists of three parts: the transient component T_t that reflects the temperature increase at the early stage of laser heating, the final temperature elevation $\bar{T}_s$ due to the laser heating, and the steady transient component $\tilde{T}_s$ that varies with time periodically. Therefore, we have $T = T_t + \bar{T}_s + \tilde{T}_s$. In the OHETS experiment, the lock-in amplifier only picks up the component that periodically varies with time. Therefore, only $\tilde{T}_s$ needs to be evaluated. $\tilde{T}_s$ results from the periodical source term $Q_0 \cdot \exp(i\omega t)$ in equation (1). When only this source term is considered, the solution to equation (1) is in the form of $\tilde{T}_s = \theta e^{i\omega t}$. Substituting this expression in equation (1), it is not difficult to find that the solution θ has the form of

$$\theta = \frac{Q_0}{\rho c_p i\omega} + C_1 e^{\sqrt{A}z} + C_2 e^{-\sqrt{A}z}, \tag{2}$$

where $A = \rho c_p \cdot i\omega/k$. To simplify the derivation expression, we take $B = Q_0/(\rho c_p i\omega)$. At $z = 0$, the wire temperature is assumed to be $T_0 e^{i\omega t}$. Consequently, C_1 and C_2 are solved as $C_1 = (T_0 - B)(1 + e^{\sqrt{AL}})$ and $C_2 = (T_0 - B)(1 + e^{-\sqrt{AL}})$.

After solving the 3D heat transfer equation in the electrode base and combining the solution with equation (2), we have

$$T_0 = \frac{U_1 B(1 + U_2)}{U_1(1 + U_2) - 1}, \tag{3}$$

$$T_1 = \frac{U_1 B}{U_1(1 + U_2) - 1}, \tag{4}$$

$$U_1 = k\sqrt{A}\cdot(1 - e^{\sqrt{AL}})/\{(1 + e^{\sqrt{AL}})\cdot[2k_b(r_0^{-1} + \sqrt{A_1})]\}, \tag{5}$$

$$U_2 = R_{tc}\cdot 2k_b(r_0^{-1} + \sqrt{A_1}), \tag{6}$$

where $A_1 = \rho_b c_{p,b} i\omega/k_b$. ρ_b, $c_{p,b}$ and k_b are the density, specific heat and thermal conductivity of the electrode base, respectively. R_{tc} is the thermal contact resistance between the wire and the base, and r_0 is the radius of the wire. Details of the derivation procedure to obtain equations (3)–(6) can be found in [6] on the 3ω experiment of single wires.

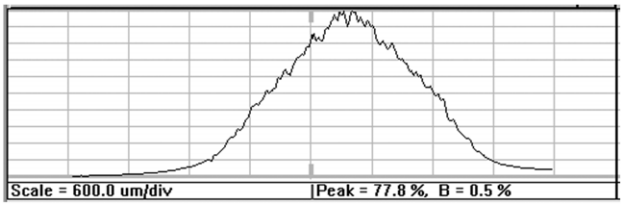

Figure 2. Measured energy distribution of the laser beam used in our experiment. In the experiment, the laser beam spot is magnified to about 10 mm in diameter.

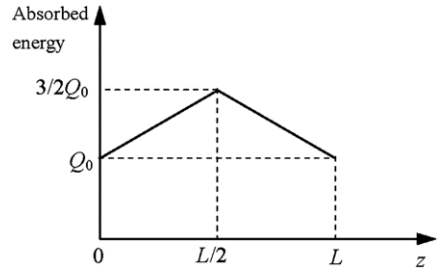

Figure 3. Hypothetical energy distribution of the laser beam used in the calculation.

We are interested in the average temperature ($\bar{\theta}$) of the wire. By integrating equation (2) along the wire, we can find $\bar{\theta}$ as

$$\bar{\theta} = \frac{1}{L/2}\int_0^{L/2}\theta\,dz = B + \frac{2}{L}\left[\frac{1}{\sqrt{A}}(C_1 e^{\sqrt{A}L/2} - C_2 e^{-\sqrt{A}L/2}) + \frac{1}{\sqrt{A}}(C_2 - C_1)\right]. \tag{7}$$

The average temperature variation $\bar{\tilde{T}}_s$ (in complex form) along the wire is calculated as

$$\bar{\tilde{T}}_s = \bar{\theta} e^{i\omega t} = \bar{\theta}_0 e^{i(\omega t + \phi)}, \tag{8}$$

where $\bar{\theta}_0$ and ϕ are the amplitude and phase of $\bar{\theta}$, respectively.

It is noticed that only the real part of $\tilde{T}_s$ is the solution to the original equation (equation (1)). Therefore, we only use the real part of $\bar{\tilde{T}}_s$ [$\bar{\theta}_0 \cos(\omega t + \phi)$] to get the ω voltage across the wire. Finally, as the product of $\bar{\theta}_0 \cos(\omega t + \phi)$ and the dc current I, the ω voltage across the wire is

$$V_\omega = \bar{\theta}_0 \cdot \frac{dR}{dT} I \cdot \cos(\omega t + \phi). \tag{9}$$

2.3. Effect of non-uniformity of the laser beam

In equation (1) as discussed above, the laser beam is assumed uniform over the entire wire while in practical situations there is a non-uniform distribution. Figure 2 shows the intensity profile of the diode laser beam ($\lambda = 809$ nm) used in our experiment. It is clear that the laser beam has a Gaussian distribution. In order to find out to what extent the phase shift of the ω signal is affected by the non-uniformity of the laser beam, the energy distribution of the laser beam is assumed linear from $z = 0$ to $z = L/2$ as shown in figure 3. This linear distribution is not intended to recover the real laser beam distribution, but to simplify the situation to understand the

effect of the non-uniformity of the laser beam. The laser energy distribution shown in figure 3 has 50% difference between the laser energy at the end and middle of the wire. This provides an extreme situation while in our experiment the laser energy distribution over the wire will be more uniform, especially for short wires irradiated with a large laser beam spot. Therefore, the effect of the non-uniformity of laser beam distribution in real experiments will be much less than the one discussed below. Considering the laser energy distribution shown in figure 3, the governing equation of the heat transfer along the wire is expressed as

$$\frac{\partial(\rho c_p T)}{\partial t} = k\frac{\partial^2 T}{\partial z^2} + Q_0[\cos(\omega t) + 1] \times \left(1 + \frac{z}{L}\right). \quad (10)$$

Following the similar derivation discussed in 2.2, we can find

$$\theta = \frac{Q_0}{\rho c_p \mathrm{i}\omega} + \frac{z/L \cdot Q_0}{\rho c_p \mathrm{i}\omega} + C_5 \mathrm{e}^{\sqrt{A}z} + C_6 \mathrm{e}^{-\sqrt{A}z}. \quad (11)$$

Using the boundary conditions to determine the constants in equation (11) and integrating equation (11) from 0 to $L/2$, the average temperature variation over the wire is

$$\bar{\theta} = \frac{1}{L/2}\int_0^{L/2} \theta \, \mathrm{d}z = \frac{5}{4}B + \frac{2}{L}\left[\frac{1}{\sqrt{A}}(C_5 \mathrm{e}^{\sqrt{A}L/2} - C_6 \mathrm{e}^{-\sqrt{A}L/2}) + \frac{1}{\sqrt{A}}(C_6 - C_5)\right], \quad (12)$$

where

$$C_5 = [(T_0 - B)\sqrt{A} \cdot \mathrm{e}^{-\sqrt{A}L/2} - B/L]/(\sqrt{A}\mathrm{e}^{\sqrt{A}L/2} + \sqrt{A}\mathrm{e}^{-\sqrt{A}L/2}), \quad (13)$$

$$C_6 = T_0 - B - C_5, \quad (14)$$

$$T_0 = \{B \cdot k\sqrt{A}(\mathrm{e}^{-\sqrt{A}L/2} - \mathrm{e}^{\sqrt{A}L/2})/(\mathrm{e}^{\sqrt{A}L/2} + \mathrm{e}^{-\sqrt{A}L/2}) - k \cdot B[1 - 1/(\mathrm{e}^{\sqrt{A}L/2} + \mathrm{e}^{-\sqrt{A}L/2})]\}\{[-2k_b/(U_2 + 1) \times (1/r_0 + \sqrt{A_1}) + k \cdot \sqrt{A}(\mathrm{e}^{-\sqrt{A}L/2} - \mathrm{e}^{\sqrt{A}L/2})/(\mathrm{e}^{\sqrt{A}L/2} + \mathrm{e}^{-\sqrt{A}L/2})]\}^{-1}. \quad (15)$$

Other coefficients in equations (13–15) are the same as those defined before. To explore how the non-uniform energy distribution influences the phase shift of the ω signal, calculation is made for a Pt wire that has the same dimensions as that used in our experiment for calibration and validation purposes. The properties of the wire and the electrode bases (copper) are summarized in table 1 [20, 21]. The thermal contact resistance takes a small value of 1.0×10^{-9} m^2 K^{-1} W^{-1}. The laser energy absorbed by unit volume of the platinum wire (Q_0) is fixed to be 3.584×10^7 W m^{-3}, which is estimated based on our experimental result. The phase shift of the voltage variation over the wire with and without considering the non-uniformity of the laser energy distribution is calculated and shown in figure 4. It is seen that at low frequencies, the non-uniformity of the laser beam has a negligible effect on the phase shift of the voltage variation. At high frequencies, a difference of about one degree is induced by the non-uniformity of the laser beam. For higher frequencies, our extended calculations show that the phase shift difference induced by the non-uniformity of the laser beam will become smaller and negligible. It needs to be pointed out that in the experiment, the low frequency signals play a major role in data fitting to determine the thermophysical properties of the material. The fitting results will be less sensitive to the phase shift at high frequencies. It is conclusive that the non-uniformity of the laser beam distribution in the OHETS experiment can be neglected. Our experimental results using Pt wires also confirm this point, and will be discussed in section 3.

Table 1. Properties of the platinum wire and copper (300 K) [21] used in the calculation.

	Platinum wire	Copper
Length (mm)	6.35	—
Density (kg m^{-3})	2.145×10^4	8.933×10^3
Specific heat (J kg^{-1} K^{-1})	133	385
Electrical resistivity[a] (ohm m)	0.1086×10^{-6}	—
Temperature coefficient of resistance α[a] (ohm K^{-1})	0.003 927	—
Thermal conductivity[a] (W m^{-1} K^{-1})	71.6	401

[a] These properties are from [20]. At 300 K, the electrical resistivity of copper is $0.106 \times 10^{-6}/[1 + (293.15 - 273.15)] \times 0.003\,927 \times [1 + (300 - 273.15) \times 0.003\,927] = 0.1086 \times 10^{-6}$ ohm m.

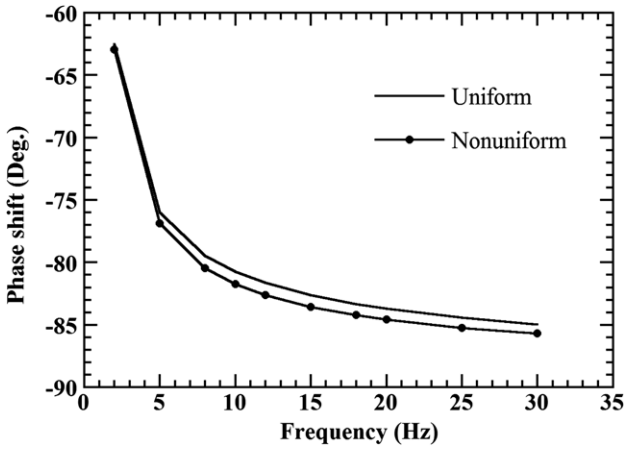

Figure 4. Phase shift of the voltage variation over a Pt wire with and without considering non-uniform energy distribution.

When considering radiation heat loss from the wire surface, a new term $-\pi DL\varepsilon\sigma(T^4 - T_{\mathrm{sur}}^4)/(\pi D^2 L/4)$ should be added to the right side of equation (1), where ε, σ are the thermal emissivity and Stefan–Boltzmann constant, respectively. T_{sur} is the surrounding temperature. As stated before, $T = T_{\mathrm{t}} + \bar{T}_{\mathrm{s}} + \tilde{T}_{\mathrm{s}}$, in steady-state $T_{\mathrm{t}} = 0$, so $T = \bar{T}_{\mathrm{s}} + \tilde{T}_{\mathrm{s}}$. Because $\tilde{T}_{\mathrm{s}} \ll \bar{T}_{\mathrm{s}}$, to the first order approximation, we have $T^4 = \bar{T}_{\mathrm{s}}^4 + 4\bar{T}_{\mathrm{s}}^3 \cdot \tilde{T}_{\mathrm{s}}$. Only the transient part $4\bar{T}^3 \cdot \tilde{T}_{\mathrm{s}}$ will affect the periodical temperature variation ($\tilde{T}_{\mathrm{s}}$). Following the similar derivation in 2.2, we only have to replace $\rho c_p \cdot \mathrm{i}\omega$ with $\rho c_p \cdot \mathrm{i}\omega + 16\varepsilon\sigma\bar{T}_{\mathrm{s}}^3/D$ in the solution developed for equation (1). The radiation effect depends on the ratio of $16\varepsilon\sigma\bar{T}_{\mathrm{s}}^3/D$ over $\rho c_p \cdot \mathrm{i}\omega$, which is detailed in [6] on the 3ω experiment of single wires. Based on the experimental conditions in this experiment, it is estimated that the radiation effect is negligible.

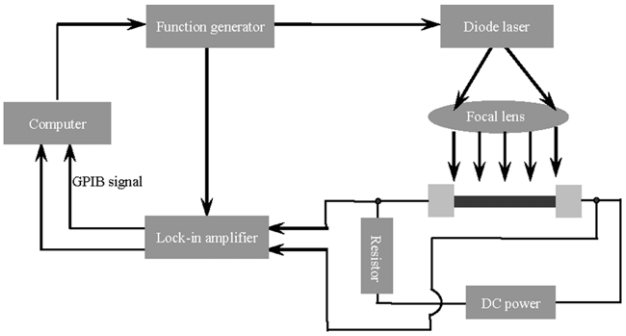

Figure 5. Schematic set-up for the OHETS experiment.

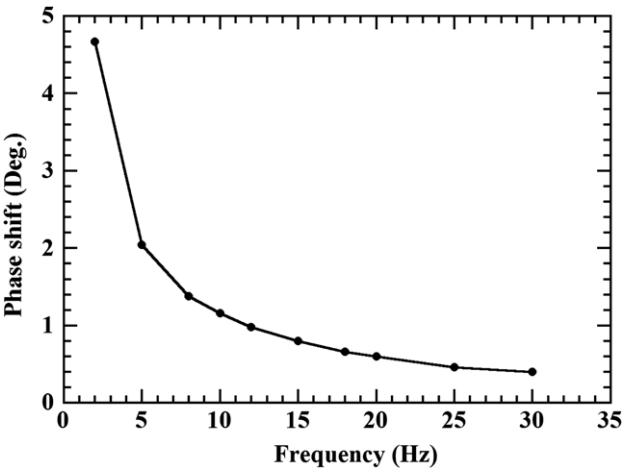

Figure 6. System time delay induced by the equipment used in the OHETS experiment.

3. Experimental details and results

3.1. Experimental set-up

Figure 5 shows the diagram of the OHETS experimental setup. An infrared diode laser ($\lambda = 809$ nm) is used in the experiment and is modulated by a function generator. The laser beam passes through a collimator and is directed by a focal lens to the to-be-measured wire. A dc voltage is applied to the thin wire. A large resistor is connected in the circuit to control the current and to satisfy the impedance requirement (over 50 Ω) of the dc power supply. A digital lock-in amplifier is used to pick up the ω signal over the thin wire, and a synchronizing signal from the same function generator is used as the lock-in amplifier's reference. In order to minimize the influence from air convection, the thin wire is housed in a vacuum chamber where the pressure is maintained at a level of 1×10^{-3} Torr. A computer is used to control the experiment for automatic data acquisition.

3.2. System calibration

In the OHETS experiment, the phase shift of the voltage variation over the wire is the parameter to measure and be used for data fitting. On the other hand, the measurement result will inevitably include some time delay induced by the equipment used in the experiment. This system time delay is calibrated by measuring the phase shift between the modulated laser beam and the synchronizing signal of the function generator. In this calibration, a photodiode, whose response time (sub-nanosecond) is far smaller than the period of the modulation signals, is chosen to detect the modulated laser beam. The measured phase shift is shown in figure 6. As shown in figure 6, this system time delay ($\phi_{\rm cal}$) is not negligible. The real phase shift between the thermal variation and the modulated laser beam is calculated as $\phi_{\rm mea} - \phi_{\rm cal}$, where $\phi_{\rm mea}$ is the raw measurement data for the voltage variation over the wire.

Table 2. Details of experimental conditions for the Pt wire and three SWCNT samples characterized in the experiment.

	Pt wire	CNT 1	CNT 2	CNT 3
Length (mm)	6.35	6.35	6.35	6.35
Resistance of sample (ohm)	1.35	90.0	443.0	392.0
DC voltage (V)	1.80	0.3	0.3	0.3
Laser power (W)	1.60	4.0	0.8	0.8
Resistance of the resistor (ohm)	99.52	99.48	99.48	99.48
$\phi_{\rm diff}$ (degree)	0.5	1.0	2.3	1.5

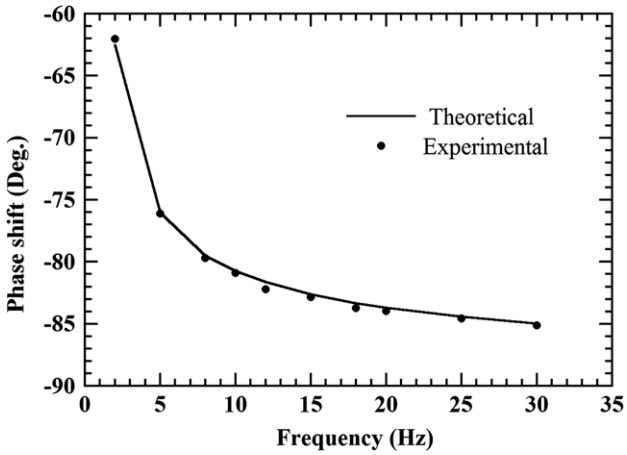

Figure 7. Phase shift as a function of the modulation frequency for the platinum wire.

In order to verify this characterization technique and the theoretical model developed in section 2, a 25.4 μm thick and 6.35 mm long platinum wire is measured. The experimental conditions, such as the applied laser power, dc voltage, and the resistor are listed in table 2. The visible size of the laser spot is around 10 mm. Figure 7 shows the fitting result in comparison with the experimental data. In the least square data fitting, the phase shift difference between the experimental data and fitting result is calculated as $\phi_{\rm diff} = \sqrt{1/j \sum_i^j (\phi_i - \phi_{{\rm theo},i})^2}$, where j, ϕ_i and $\phi_{{\rm theo},i}$ denote the number of experimental frequencies, experimental phase shift and fitting result, respectively. Figure 8 shows how sensitive the fitting result is with respect to the phase shift. As shown in figure 8, the minimum $\phi_{\rm diff}$ is found to be 0.3°. In the experiment, the uncertainty of the measured phase shift is less 0.5°. Based on this criterion, if $\phi_{\rm diff} = 0.5°$ is chosen as the experimental uncertainty, the thermal conductivity k is found to be $71.4^{+3.7}_{-3.4}$ W m^{-1} K^{-1}, close to the literature value of 71.6 W m^{-1} K^{-1} [21].

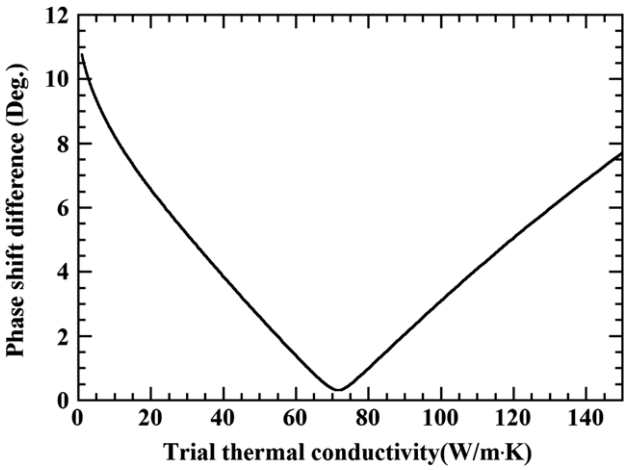

Figure 8. Phase shift difference between the measurement data and fitting results versus trial thermal conductivity for the platinum wire.

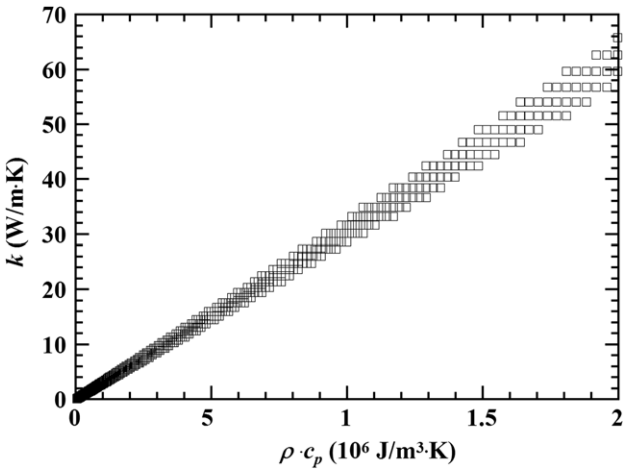

Figure 10. Thermal conductivity versus $\rho \cdot c_p$ for the first SWCNT bundle.

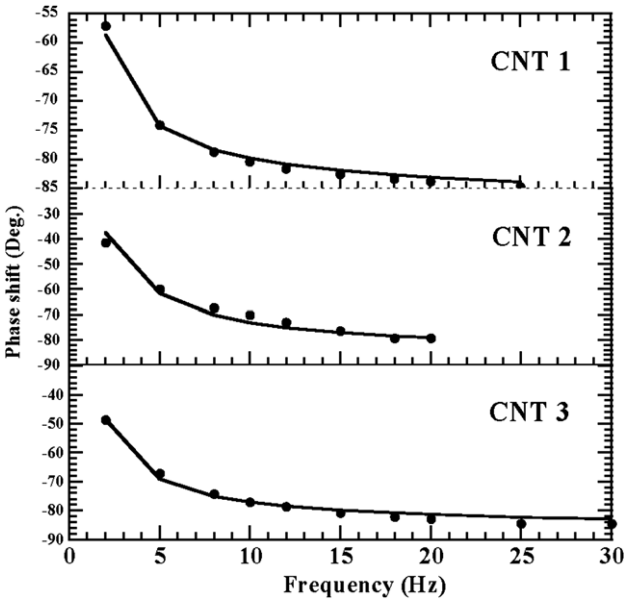

Figure 9. The measured phase shift versus the fitting results for the three SWCNT bundles. ——: theoretical calculation; · · · · · ·: experimental data.

3.3. Thermal characterization of SWCNT bundles

In this section, bundles consisting of SWCNTs are measured using the established OHETS technique and the developed solution. Centimetres long ropes of well-aligned SWCNTs were synthesized using an H_2/Ar arc discharge method. The synthesis process is described in detail in the work of Liu *et al* [22]. In brief, Ar and H_2 gases were introduced into a vacuum chamber as buffer gases. The cathode was a graphite rod with the tip sharpened, and the anode was a graphite cylinder with holes filled by evenly dispersed graphite powder, Fe–Ni–Co catalyst, and a sulfur-containing growth promoter. An angle between the axes of the two electrodes was set as 30–50°. When an electric arc is initiated, the SWCNT strands can be obtained on the collectors installed in the reaction chamber.

In the experiment, the SWCNT bundle is connected between two copper electrodes using silver paste. Table 2 shows the length and resistance of the three SWCNT bundles measured in the experiment. The laser power, dc voltage and resistor used in the experiment are also summarized in table 2. The typical thickness/diameter of the SWCNT bundles is measured to be around 100 μm. Under this condition, the effect of radiation heat loss from the bundle surface will have a negligible effect on the measured ω signals [6]. The thermal conductivity of the SWCNT bundle becomes difficult to determine based on the experimental data due to the lack of data about the density and specific heat of the SWCNT bundles. Instead, the thermal diffusivity of the sample is characterized based on the phase shift of the ω signal.

Figures 9(*a*)–(*c*) show the fitted phase shift versus the experimental data for the three samples in which the SWCNTs have sound alignment along the wire axis. For the three samples measured in the experiment, different values of $\rho \cdot c_p$ are used to fit the thermal conductivity. Although a large number of thermal conductivity and $\rho \cdot c_p$ combinations can fit the experimental data well, their ratio-thermal diffusivity remains at a certain value for each sample. Their thermal diffusivities are fitted to be $2.98^{+0.3}_{-0.2} \times 10^{-5}\,\mathrm{m^2\,s^{-1}}$, $4.41^{+0.4}_{-0.3} \times 10^{-5}\,\mathrm{m^2\,s^{-1}}$ and $6.64^{+0.4}_{-0.2} \times 10^{-5}\,\mathrm{m^2\,s^{-1}}$, respectively. For different samples, ϕ_{diff} is fixed at different value shown in table 2, which can both guarantee best agreement between experiment and theoretical model and a large number of thermal conductivity and $\rho \cdot c_p$ combinations. Figure 10 shows combinations of the thermal conductivity and $\rho \cdot c_p$ for the first SWCNTs bundle which has the thermal diffusivity of $2.98^{+0.3}_{-0.2} \times 10^{-5}\,\mathrm{m^2\,s^{-1}}$. For this sample, when ϕ_{diff} is less than 1.0°, the $\rho \cdot c_p$ and k combination will be recorded and plotted in figure 10. It is evident that the $k \sim \rho \cdot c_p$ curve is a linear line within the experimental uncertainty, confirming that there is only one thermal diffusivity to fit the experimental result. Based on the obtained experimental results, the thermal diffusivity of the three samples is in the same order. The difference among them is probably attributed to different alignment of the tube bundles and tube–tube interaction. The average value of the thermal diffusivity of above stated three different SWCNT samples is around $4.68 \times 10^{-5}\,\mathrm{m^2\,s^{-1}}$.

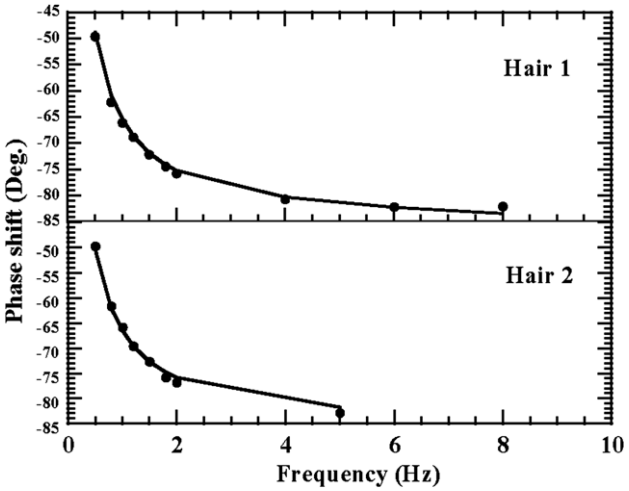

Figure 11. The measured phase shift versus the fitting results for human hair. ——: theoretical calculation; · · · · · ·: experimental data.

3.4. Thermal characterization of human hair and cloth fibre with coated Au film for electrical thermal sensing

For non-conductive wires, the OHETS technique cannot be directly applied since no electrical thermal sensing is feasible. To sense the periodical temperature variation in the wire, one side of the wire is coated with a very thin (∼2 nm) Au film. The modulation frequency (ω) of the laser is carefully selected to make the thermal diffusion length $\mu = \sqrt{2\alpha/\omega}$ in the wire (α: thermal diffusivity of the wire) much larger than the wire diameter D. As a result, it is physically reasonable assuming that the wire has a uniform temperature distribution over its cross-section. Therefore, the temperature of the metallic coating represents that of the wire. For human hair, the sample was coated in the sputter coating machine first. The measured samples were cut from the coated hair and connected between two Cu electrodes using silver paste. After connection was made, hair 1 (2.718 mm long) has a resistance of 218 ohms; hair 2 (4.013 mm long) has a resistance of 512 ohms. A resistor (1 kΩ) was connected in series with the hair samples and a laser energy of 1.9 W was used to run the measurement for each sample. For the dc voltage, 0.3 V was applied on hair 1 and the resistor and 0.2 V was applied on hair 2 and the resistor. Figure 11 displays the measured phase shift and the data fitting result for the human hair. Our experiment shows that the thermal diffusivity of the two human hair samples is $1.94 \times 10^{-6}\,\mathrm{m^2\,s^{-1}}$ and $4.13 \times 10^{-6}\,\mathrm{m^2\,s^{-1}}$ for hair 1 and 2, respectively. The thermal diffusivity difference between these two samples probably is due to the different growing positions of the hair on the head and different growing period, although the two hair samples are from the same person, a 25-year old male graduate student in our department.

For the cloth fibres- poly (ethylene terephthalate) studied in this work, the SEM picture of one fibre with coated Au film is shown in figure 12. This is only a sample for the SEM test, not the one measured to obtain the thermal diffusivity as shown in figure 13. For the sample preparation, the cloth fibre with a diameter of 10 μm was carefully suspended between two Cu electrodes about 1.727 mm apart. Silver paste was used to strengthen the mechanical contact. After the bridge was made, the sample was put in a sputter coating machine

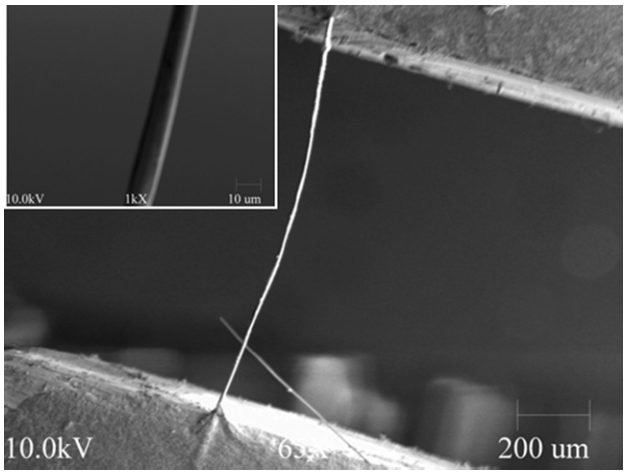

Figure 12. One of the coated cloth fibres studied in this work.

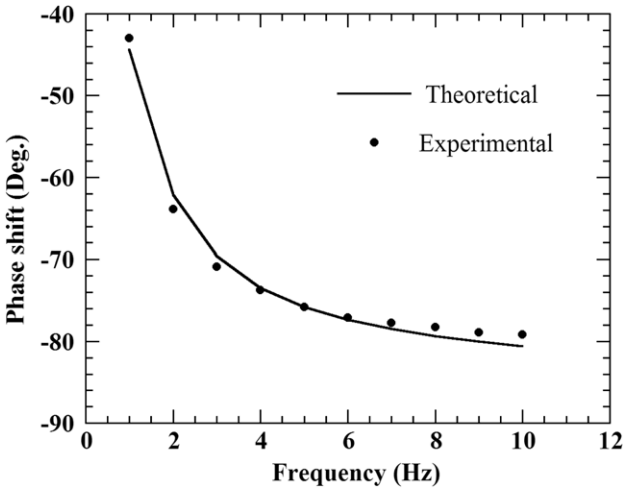

Figure 13. The measured phase shift versus the fitting results for the cloth fibre.

to coat a very thin Au film (∼nm) on one side of the cloth fibre. Again, the silver paste was applied on the edges of Cu electrodes to improve the electrical contact between the coated fibre and electrodes. After the Au film was coated, the bridge has a resistance of about 400 Ω. A resistor of 1 kΩ was put in series with this bridge and a 0.04 V dc voltage was applied on the bridge and resistor. For laser heating, the maximum output (4.0 W) of our diode laser was used. Based on phase shift fitting, the thermal diffusivity of the cloth fibre is determined as $1.89 \times 10^{-6}\,\mathrm{m^2\,s^{-1}}$. The phase shift fitting result is shown in figure 13.

3.5. Discussion about the experiment

During the measurement, the temperature of the sample will increase. To calculate or measure the exact temperature rise becomes difficult due to the small size of the sample and lack of knowledge about the thermal conductivity of the sample and laser beam absorption. On the other hand, some first order estimation can still be done to give a general idea. For example, in our experiment, the estimated average temperature increase of the platinum wire due to electrical and laser heating is 11 °C. Our estimation is based on one-dimensional heat transfer in the

wire and the experimental conditions used in the measurement. All the electrical heating and an assumed 10% laser beam absorption is considered to obtain this average temperature increase. For other materials measured in this work, the lack of precise properties places difficulty on the estimation. Our estimation suggests that their temperature rise is not beyond 50 °C.

In the measurement of non-conductive wires, the effect of Au coating should be considered. The thermal conductance (G_f) of the thin film coating is defined as

$$G_f = A_f k_f / L, \tag{16}$$

where k_f , A_f are the thermal conductivity and cross-sectional area of the film, respectively. It is noted that k_f can be much different from the bulk material's value due to the unique structure and small thickness of the thin film coating. In addition, the cross-sectional area (A_f) of the thin film cannot be directly calculated using $A_f = A_e - A_w$, where A_e and A_w are the cross-sectional area of wire with and without Au coating. This is because A_e and A_w could be close to each other attributed to the nanometre-order thickness of the thin film coating. As a result, $A_f = A_e - A_w$ could induce large uncertainty in evaluating the cross-sectional area of the thin film.

In our work, G_f is evaluated using the Wiedemann–Franz Law, which relates the thermal conductivity (k) of metal to its electrical conductivity (σ) as $L_{Lorenz} = k/(\sigma T)$. The Lorenz number L_{Lorenz} for Au has weak dependence on temperature: $2.35 \times 10^{-8}\,W\,\Omega\,K^{-2}$ at 0 °C and $2.40 \times 10^{-8}\,W\,\Omega\,K^{-2}$ at 100 °C [23]. Based on the Wiedemann–Franz Law, the thermal conductance of the thin film coating can be readily calculated based on the measured electrical resistance of the wire as

$$G_f = L_{Lorenz} T / R. \tag{17}$$

In the experiment, the measured thermal diffusivity (α_e) is the combined contribution from the wire and Au coating, which can be expressed as

$$\alpha_e = \frac{k(1-\beta) + k_f \beta}{\rho c_p (1-\beta) + \rho_f c_{p,f} \beta}, \tag{18}$$

where ρ_f and $c_{p,f}$ are the density and specific heat of the Au coating. $\beta = A_f/A_e$ is the cross-sectional area ratio of Au coating. Since $\beta \ll 1$, we have $\rho_f c_{p,f} \beta \ll \rho c_p (1-\beta)$ and $1 - \beta \cong 1$. Equation (18) can be simplified as

$$\alpha_e = \frac{k + k_f \beta}{\rho c_p}. \tag{19}$$

Considering equations (16) and (17) and $\beta = A_f/A_e$, we can get $k_f \beta = (L_{Lorenz} \cdot T/R) \cdot L/A_w$. So the real thermal diffusivity of the wire (α) is calculated as

$$\alpha = \alpha_e - \frac{L_{Lorenz} \cdot T \cdot L}{R \cdot A_w \cdot \rho \cdot c_p}. \tag{20}$$

Following this amendment and using the density and specific heat [24] of polyester ($\rho = 1.368 \times 10^3\,kg\,m^{-3}$, $c_p = 1.2 \times 10^3\,J\,kg^{-1}\,K^{-1}$), the thermal diffusivity of the measured cloth fibre is calculated as $1.65 \times 10^{-6}\,m^2\,s^{-1}$. For human hair, we find that the Au coating has a negligible effect. It needs to be pointed out that the resistance (R) used in equation (20) has some contribution from contact electrical resistance at the ends of the wire. The real electrical resistance of the Au coating will be smaller than the value measured in the experiment. Therefore, it is anticipated the real thermal diffusivity of the cloth fibre will be smaller than the value reported above. To further reduce the effect of the Au coating on the measured thermal diffusivity, a very thin coating (meaning large electrical resistance) is preferred.

In the experiment, the temperature increase of the wire will change its diameter and length. Considering the fact that the thermal expansion coefficient of materials usually is in the order of $10^{-5}\,°C^{-1}$, the moderate temperature increase (less than 50 °C) of the wire will result in a less than 0.1% change in its diameter and length. In phase shift fitting, the diameter of the wire is not critical, and has a negligible effect. In the solution developed in this work, the length (L) of the wire appears in the form of $L/\sqrt{\alpha/\omega}$. Due to the combined electrical and optical heating, the induced uncertainty in the fitted thermal diffusivity will be less than 0.2%. Therefore, it is conclusive that the heating-induced size change of the sample will have a negligible effect on the fitting result. In the experiment, the accuracy for length measurement usually is high, in the order of 5% or better. Therefore, the uncertainty of the fitted thermal diffusivity due to length measurement will be less than 10%.

4. Conclusion

In this work, a technique based on OHETS was developed to characterize the thermal transport in one-dimensional micro/nanostructures. The effect of the non-uniformity of the laser beam irradiating the wire was studied to confirm that the non-uniformity of the laser beam had a negligible effect on the measured phase shift for micro-thick wires. Applying this technique, the thermal conductivity of a platinum wire was measured to be $71.4\,W\,m^{-1}\,K^{-1}$, agreeing well with the reference value. We have measured the thermal diffusivity of SWCNT bundles of different thicknesses. The average thermal diffusivity for the three SWCNT samples was $4.68 \times 10^{-5}\,m^2\,s^{-1}$, which is much smaller than that of graphite in the layer direction. Applying the OHETS technique, the thermal diffusivities of microscale non-conductive wires (human hair and cloth fibre) were also characterized successfully.

Acknowledgments

This work was supported by NSF (CTS: 0400458), Nebraska Research Initiative, the MURI Grant from ONR, and Layman Award of the University of Nebraska-Lincoln (UNL). SWCNT bundles were provided by Chang Liu and Huiming Cheng from the Shenyang National Laboratory for Materials Science, Chinese Academy of Sciences. The authors really appreciate this strong support. Support from Dr Dennis Alexander and Haifeng Zhang of the Electrical Engineering Department at UNL for measuring the laser beam energy distribution is very much appreciated.

References

[1] Paddock C and Eesley G 1986 *J. Appl. Phys*. **60** 285–90
[2] Cahill D and Pohl R 1987 *Phys. Rev.* B **35** 4067–73
[3] McGahan W and Cole K 1992 *J. Appl. Phys.* **72** 1362–73
[4] Hu H, Wang X and Xu X 1999 *J. Appl. Phys*. **86** 3953–8
[5] Lu L, Yi W and Zhang D L 2001 *Rev. Sci. Instrum.* **72** 2996–3003
[6] Vellelacheruvu P 2006 Experimental research on thermal transportation in individual one-dimensional micro/nano structure *MS Thesis* University of Nebraska–Lincoln (available upon request)
[7] Kim P, Shi L, Majumdar A and McEuen P L 2001 *Phys. Rev. Lett.* **87** 215502:1–4
[8] Shi L, Li D, Yu Ch, Jang W, Kim D, Yao Z, Kim P and Majumdar A 2003 *J. Heat Transfer* **125** 881–8
[9] Dresselhaus M S, Dresselhaus G and Eklund P C 1996 *Science of Fullerenes and Carbon Nanotubes* (San Diego: Academic)
[10] Hone J, Whitney M, Piskoti C and Zettl A 1999 *Phys. Rev.* B **59** R2514–6
[11] Hone J, Llaguno M C, Nemes N M, Johnson A T, Fischer J E, Walters D A, Casavant M J, Schmidt J and Smalley R E 2000 *Appl. Phys. Lett.* **77** 666–8
[12] Vavro J, Llaguno M C, Satishkumar B C, Luzzi D E and Fischer J E 2002 *Appl. Phys. Lett.* **80** 1450–2
[13] Yu C, Shi L, Yao Z, Li D and Majumdar A 2005 *Nano Lett.* **5** 1842–6
[14] Xie S, Li W, Pan Z, Chang B and Sun L 2000 *J. Phys. Chem. Solids* **61** 1153–8
[15] Yi W, Lu L, Zhang D, Pan Z and Xie S 1999 *Phys. Rev.* B **59** R9015–8
[16] Zhang H L, Li J-F, Yao K F and Chen L D 2005 *J. Appl. Phys.* **97** 114310
[17] Wang X, Zhong Z and Xu J 2005 *J. Appl. Phys.* **97** 064302:1–5
[18] Choi T Y, Poulikakos D, Tharian J and Sennhauser U 2005 *Appl. Phys. Lett.* **87** 013108:1–3
[19] Brown E, Hao L, Gallop J C and Macfarlane J C 2005 *Appl. Phys. Lett.* **87** 023107:1–3
[20] Weast R C, Astle M J and Beher W H 1983–84 *Handbook of Chemistry and Physics* 64th edn (Boca Raton, FL: CRC Press) F-125
[21] Incropera F and Dewitt D 2002 *Heat and Mass Transfer* 5th edn (New York: Wiley)
[22] Liu C, Cheng H M, Cong H T, Li F, Su G, Zhou B L and Dresselhaus M S 2000 *Adv. Mater.* **12** 1190–2
[23] Kittel C 1976 *Introduction to Solid State Physics* 5th edn (New York: Wiley) p 178
[24] Olenka L, Da Silva E N, Santos W L F, Muniz E C, Rubira A F, Cardoso L P, Medina A N, Miranda L C M, Baesso M L and Bento A C 2001 *J. Phys. D: Appl. Phys.* **34** 2248–54